

Article

High-Level Vibration for Single-Frequency and Multi-Frequency Excitation in Macro-Composite Piezoelectric (MFC) Energy Harvesters, Nonlinearity, and Higher Harmonics

Majid Khazaei ^{1,2} 

¹ Department of AAU Energy, Aalborg University, Pontopidanstraede 111, 9220 Aalborg, Denmark; mad@energy.aau.dk

² School of Biomedical Engineering, Faculty of Engineering, The University of Sydney, NSW 2000, Australia

Abstract: This paper presents an extensive experimental investigation to identify the influence of signal parameters on a piezoelectric harvester's performance. A macro-fibre composite energy harvester was studied as an advanced, flexible, high-performance energy material. Gaussian white noise, and single-frequency and multi-frequency excitation were used to investigate nonlinearity and multiple-frequency interactions. Using single low and high frequencies, we identified the nonlinearity of the harvester's vibration. Multi-frequency excitation with a series of low-to-high-frequency harmonics mimicked the practical vibration signal. Under such multi-frequency excitation, the harvester's nonlinear behaviour was studied. Finally, the interaction effects among multiple frequencies were identified. The results show that under pure resonant excitation, high-level vibration led to high-level mechanical strain, which caused nonlinear vibration behaviour. Moreover, it was shown that the different harmonics excited the various structure bending modes, which caused the nonlinearity of multi-frequency excitation. The first four harmonics of the real-time signal were important. The experimental results emphasise the resonant nonlinearity and interactions of multi-frequency excitation effects.



Citation: Khazaei, M. High-Level Vibration for Single-Frequency and Multi-Frequency Excitation in Macro-Composite Piezoelectric (MFC) Energy Harvesters, Nonlinearity, and Higher Harmonics. *Micromachines* **2023**, *14*, 1.

<https://doi.org/10.3390/mi14010001>

Academic Editors: Liang Wang and Dalius Mažeika

Received: 15 November 2022

Revised: 10 December 2022

Accepted: 14 December 2022

Published: 20 December 2022



Copyright: © 2022 by the author. Licensee MDPI, Basel, Switzerland. This article is an open access article distributed under the terms and conditions of the Creative Commons Attribution (CC BY) license (<https://creativecommons.org/licenses/by/4.0/>).

Keywords: piezoelectric; real-time vibration; random signal; white noise; nonlinearity

1. Introduction

Piezoelectric materials with electrical-to-mechanical conversion abilities are alternatives to power electronic devices, as they utilise the often-wasted electrical energy. Piezoelectric Vibration Energy Harvesting (PVEH) has found industrial [1] and bio-related [2] applications. By moving toward self-powered electronics with PVEH, electronic devices and biomedical sensors/actuators can be installed in inaccessible areas, such as in vivo or remote areas, using the often-wasted available energy [3].

Practical vibration signals from machines or the environment are often random, multi-frequency signals. Despite extensive PVEH from practical vibrations [4,5], a laboratory-controlled sinusoidal input is typically used as an excitation signal, which is different from real-time vibration systems, as real-time vibration signals are stochastic. Real-time randomness may affect the efficacy of piezoelectric harvester optimisation practices [6], emphasising the importance of multi-frequency vibration analysis of piezoelectric energy harvesters (PEHs). Some studies have analysed PEHs using random vibration methods, such as white noise [7] and Gaussian-coloured noise [8]. Moreover, PVEH using wind force, as another familiar environmental energy source, entails randomness, which has been experimentally investigated [9]. These studies often focus on the PEH output without properly focusing on different excitation frequencies and multi-modal beam models. In PVEH, the frequency and amplitude of the vibration source are prominent parameters of the output power of a PEH [10,11]. The PEH maximum voltage is a vibration signal with an excitation frequency close to the natural frequency [12]. This process is called frequency

matching [13,14], and many studies have presented good frequency matching [15] or broadband frequency matching [16] techniques. The vibration amplitude is another vital element that impacts the output power. According to the typical linear models, PEH power depends on the square of the amplitude of the external sinusoidal vibration [17,18].

Mechanical strain is directly linked to the electrical charge flow in a piezoelectric material. In other words, piezoelectric strain corresponds to electrical energy generation. Previous studies have pointed to the nonlinearity of PEH performance under high-level single-frequency resonant excitation [19]. The nonlinear effect is more significant when the beam is more flexible due to specific boundary conditions [20]. In the clamped–free beam, the most used PVEH configuration, the strain is non-uniform, and the clamped-end region has the maximum strain over the whole volume [16]. Thus, the piezoelectric beam experiences large strain in this configuration. A high strain level, especially under resonant clamped–free excitation, causes a nonlinear effect on the PEH; however, previous studies have not presented a comprehensive frequency-spectrum analysis of high-level vibrations.

PVEH is a multidisciplinary research area closely connected to vibration characteristics. Yet, many vibrational phenomena, such as nonlinearity and multi-frequencies, should be addressed. Modelling literature studies typically use single-frequency and linear assumptions [3,21]. In contrast, there is a lack of practical and nonlinear vibration signal analysis. The unmet goals include comprehensively analysing PEHs subjected to multi-frequency vibration signals, the interaction effects of different frequencies, the signal vibration randomness, and high-level vibrations. Such comprehensive analysis would provide an accurate energy estimation of the practical vibration sources and assess the current linear methods regarding real-time vibration signals. The present study introduces a deep experimental work on vibration signals with randomness and multi-frequencies. The effects of increasing the vibration level of different single-frequency and multi-frequency signals were studied. Moreover, the interaction effects of the different vibration modes were analysed. These innovative investigations significantly enrich the PVEH knowledge of modelling and output power estimation.

The work of this manuscript is categorised as follows: Section 2 discusses the need for multi-frequency analysis with a real-time vibration signal demonstration. A linear modelling technique is presented in Section 3 for natural frequency estimation. Moreover, the model for natural frequency estimation was validated with experimental tests, as shown in Section 4. Section 5 deals with the results and discussion, including the randomness effect, the effects of increasing the vibration level of single-frequency and multi-frequency vibrations, and the interaction effects of multi-modal vibrations on a PEH. Section 6 presents the concluding remarks and the proposed future works. The comparisons of high-level vibrations of single-frequency and multi-frequency vibration signals show the high-strain-level nonlinearity of the PEH. In addition, the interaction effects among different vibration modes can be significant.

2. The Need for Multi-Frequency Harmonic Analysis

Practical vibration sources are random vibration signals comprising a series of harmonic signals. The Fourier Transform (FT) of a time-domain vibration signal demonstrates the frequency information of the vibration source. Therefore, a full-range frequency analysis is required for energy harvesting power estimation. As a practical example, the water pump acceleration signal of a running water pump with rotation speed $\Omega = 2970$ rpm ($\Omega \approx 49.5$ Hz) is shown in Figure 1a [22]. This acceleration signal is influenced by the roller bearing elements and structural elements, which affect the FT peak amplitudes due to factors such as bearing ball diameter and number of balls [23,24]. This acceleration signal is not purely harmonic and consists of harmonic multipliers of Ω , according to the FT signal shown in Figure 1b. In the zoomed-in view of the FT signal, the four dominant frequencies are shown and marked with $1 \times \Omega$, $2 \times \Omega$, $3 \times \Omega$, and $4 \times \Omega$.

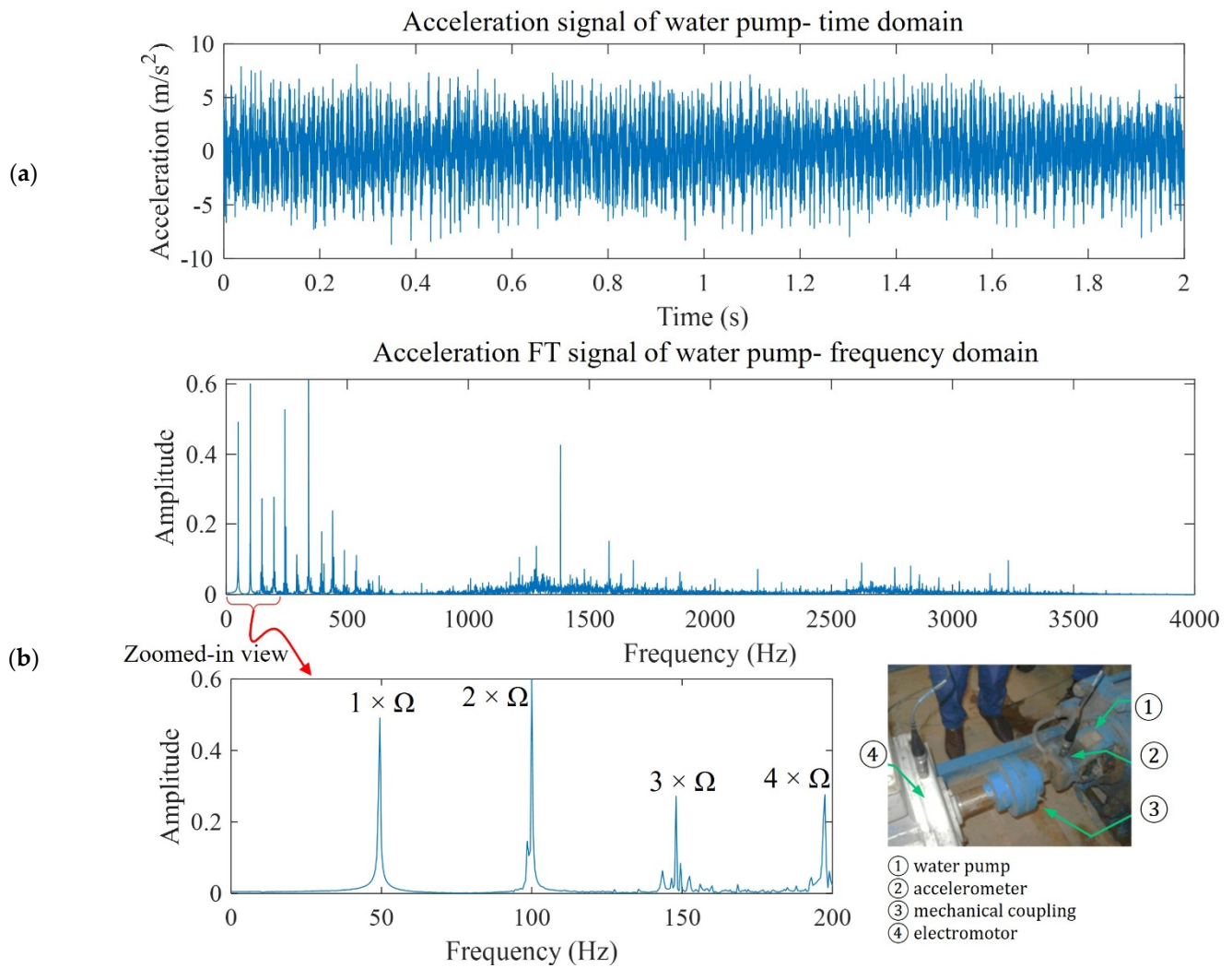


Figure 1. Real example of vibration from an operation machine: (a) acceleration and (b) frequency spectra of vibration signal from a water pump during operation.

A common assumption in piezoelectric harvester analysis is the single-mode assumption, which simplifies modelling by only considering a frequency range around the fundamental harvester frequency. Analytical modelling studies are often simplified for single-frequency harmonic vibrations, but practical vibration signals are not single-frequency harmonics. High-frequency harmonics may excite a harvester's high-vibration modes. Since an electrode covers the whole piezoelectric surface, electrical charge cancellation may be experienced in multi-vibration modes. Therefore, a full-range frequency analysis is needed to assess the high-frequency harmonics and interaction effects among high frequencies.

Moreover, most analytical models present a linear model for energy harvesting power estimation. The linear model assumes a linear relationship between input acceleration and output voltage. Nevertheless, assessing linearity under conditions of multiple vibration frequencies is difficult due to different vibration mode shapes.

3. Closed-Form Solutions for Mechanical and Electrical Responses

a_n are the sampled acceleration signal measurements of acceleration function $a(t)$. To obtain the closed-form solutions under this general load, the acceleration is represented by a series of harmonic functions using the Fast Fourier Transform (FFT).

$$A_i = \sum_{n=0}^{N-1} a_n e^{-j \frac{2\pi i n}{N}} \tag{1}$$

where A_i is the external acceleration FFT and N is the number of sampled measurement data.

For the vibration solution of the harvester, the piezoelectric beam deformation is denoted by

$$w(x, t) = \sum_{r=1}^{\infty} \phi_r(x) \eta_r(t) \tag{2}$$

where $\phi_r(x)$ is the displacement-dependent function (beam mode shapes) and $\eta_r(t)$ is the time-dependent mechanical deformation function.

The electromechanical equations of a piezoelectric unimorph without tip mass are given by [15]

$$\ddot{\eta}_r(t) + 2\zeta_r \omega_r \dot{\eta}_r(t) + \omega_r^2 \eta_r(t) + Y_r V_R(t) = \sigma_r a_n \tag{3}$$

$$C_P \dot{V}_R(t) + (1/R) V_R(t) - \Lambda_r \dot{\eta}_r(t) = 0 \tag{4}$$

where the parameters are given in Table 1. The unimorph parameters are shown in Figure 2.

Table 1. Parameters of the unimorph harvesting model.

	Definition	Formula		Parameter
ω_r	Natural frequency	$(\lambda_r L)^2 \sqrt{\frac{YI}{m^* L^4}}$	L	Beam length (m)
YI	Beam stiffness		b	Beam width (m)
m^*	Mass per unit length	$b(\rho_p h_p + \rho_s h_s)$	h	Layer thickness (m)
λ_r	Natural frequency coefficient, 1.875, 4.694, 7.885		ρ	Density (kg/m ³)
Y_r	Piezoelectric energy conversion modal coefficient	$\mathcal{P} \left(\frac{d\phi_r(x)}{dx} \Big _{x=L} \right)$	Y	Elastic modulus (Pa)
\mathcal{P}		$-\frac{\bar{e}_{31} b}{2h_p} [Z_c^2 - Z_b^2]$	$\bar{\epsilon}_{33}$	Permittivity (F/M)
Λ_r	Piezoelectric reverse energy conversion modal coefficient	$-\frac{\bar{e}_{31} (h_p + h_s) b}{2} \left(\frac{d\phi_r(x)}{dx} \Big _{x=L} \right)$	R	Electrical load (Ω)
C_P	Piezoelectric capacitance	$\frac{\bar{\epsilon}_{33} b L}{h_p}$	Z_a	Z-distance of neutral axis
$\phi_r(x)$	Harvesting beam mode shapes	$\chi_r [\cosh(\lambda_r x) - \cos(\lambda_r x)] + \alpha_i [\sinh(\lambda_r x) - \sin(\lambda_r x)]$	Z_b	Z-distance: piezo-bottom to neutral axis
			Z_c	Z-distance: neutral axis to the top
			Subscript p	Piezoelectric layer
			Subscript s	Substrate layer

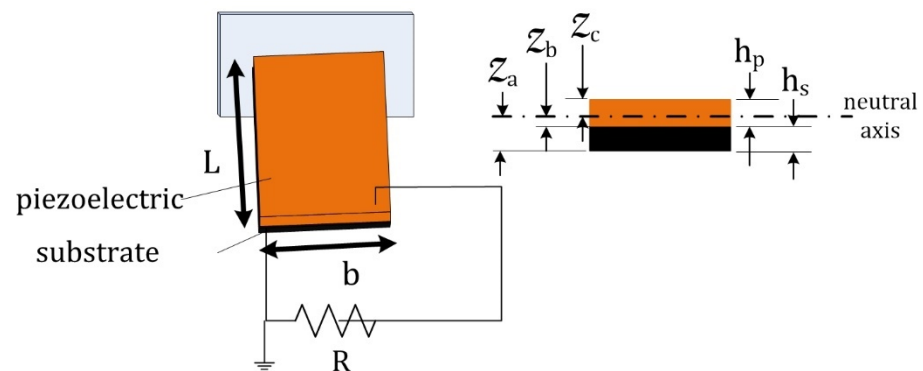


Figure 2. Piezoelectric sample with dimensions.

Assuming a linear framework, mechanical displacement $\eta_r(t)$ and output voltage $V_R(t)$ are the summation of the outputs from each harmonic Ω_i , starting from $i = 0$ to $+\infty$. Individual harmonic components are denoted with $\bar{\eta}_{r, \Omega_i}$ and \bar{V}_{R, Ω_i} , respectively. Therefore, the overall mechanical vibration and electrical responses are

$$\eta_r(t) \cong \Delta\Omega \sum_{i=0}^{N-1} \bar{\eta}_{r, \Omega_i} \cdot e^{j\Omega_i t} \tag{5.a}$$

$$V_R(t) \cong \Delta\Omega \sum_{i=0}^{N-1} \bar{V}_{R, \Omega_i} \cdot e^{j\Omega_i t} \tag{5.b}$$

where $\bar{\eta}_{r, \Omega_i}$ is the mechanical response and \bar{V}_{R, Ω_i} is the piezoelectric voltage response due to a nominal excitation harmonic with Ω_i frequency. Note that the over-bar indicates the magnitude.

For obtaining $\bar{\eta}_{r, \Omega_i}$ and \bar{V}_{R, Ω_i} , the harmonic solution analysis of the piezoelectric energy harvester differential is carried out [25], as the steady-state relationships can be given by

$$\left(\omega_r^2 - \Omega_i^2 + j2\zeta_r\omega_r\Omega_i\right)\bar{\eta}_{r, \Omega_i} + \gamma_r\bar{V}_{R, \Omega_i} = \sigma_r A_i \tag{6.a}$$

$$\left(\frac{1}{R} + jC_P\Omega_i\right)\bar{V}_{R, \Omega_i} = \sum_{r=1}^{\infty} j\Omega_i\Lambda_r\bar{\eta}_{r, \Omega_i} \tag{6.b}$$

Eliminating mechanical response $\bar{\eta}_{r, \Omega_i}$ between Equations (6.a) and (6.b), the output voltage can be expressed as

$$\bar{V}_{R, \Omega_i} = A_i \left| \frac{\frac{1}{m^*}j\Omega_i \sum_{r=1}^{\infty} \Lambda_r\sigma_r \frac{1}{\omega_r^2 - \Omega_i^2 + j2\zeta_r\omega_r\Omega_i}}{\frac{1}{R} + jC_P\Omega_i + j\Omega_i \sum_{r=1}^{\infty} \frac{\Lambda_r\gamma_r}{\omega_r^2 - \Omega_i^2 + j2\zeta_r\omega_r\Omega_i}} \right| \tag{7}$$

Finally, the total voltage generation is calculated as

$$\bar{V}_R \cong \Delta\Omega \left| \sum_{i=0}^{N-1} \bar{V}_{R, \Omega_i} \right| = \Delta\Omega \left| \sum_{i=0}^{N-1} A_i \frac{\frac{1}{m^*}j\Omega_i \sum_{r=1}^{\infty} \Lambda_r\sigma_r \frac{1}{\omega_r^2 - \Omega_i^2 + j2\zeta_r\omega_r\Omega_i}}{\frac{1}{R} + jC_P\Omega_i + j\omega_i \sum_{r=1}^{\infty} \frac{\Lambda_r\gamma_r}{\omega_r^2 - \Omega_i^2 + j2\zeta_r\omega_r\Omega_i}} \right| \tag{8}$$

The output power is calculated as

$$\bar{P}_R = \frac{\bar{V}_R^2}{R} \cong \frac{\Delta\Omega^2}{R} \left(\left| \sum_{i=0}^{N-1} A_i \frac{\frac{1}{m^*}j\Omega_i \sum_{r=1}^{\infty} \Lambda_r\sigma_r \frac{1}{\omega_r^2 - \Omega_i^2 + j2\zeta_r\omega_r\Omega_i}}{\frac{1}{R} + jC_P\Omega_i + j\omega_i \sum_{r=1}^{\infty} \frac{\Lambda_r\gamma_r}{\omega_r^2 - \Omega_i^2 + j2\zeta_r\omega_r\Omega_i}} \right| \right)^2 \tag{9}$$

This power conversion term is frequency and load dependent, in addition to being dependent on the material and geometrical properties.

Equation (9) contains essential information:

- (1) The total output power is calculated using two series over the frequency range and the modal mode shapes for general input acceleration. Therefore, parameters such as γ_r and Λ_r are mode-shape dependent, in addition to being dependent on the external frequency, which is Ω_i . The interaction between the external excitation frequency and the mode shapes is a complex research object, specifically when an electrode covers the piezoelectric layer.
- (2) Moreover, there is a linear relationship between the output power and the external square acceleration amplitude. This linear dependency over different frequencies needs to be researched, since excitation and modal mode interactions can be nonlinear.

This paper tackles the above two research questions.

4. Experimental Setup and Initial MFC Harvester Characterisation

4.1. Experimental Setup

Figure 3a shows the test rig for all the experimental measurements. Two aluminium base plates connected a B&K shaker to the piezoelectric sample, tightened with four bolts. The amplifier was controlled with a National Instruments NI 9263 module, which generated analogue voltage signals. A KEPCO BOP 100-10MG amplifier amplified the signals and powered the shaker. The piezoelectric harvester output wires were connected across a resistive load of resistance R . A Data Acquisition (DAQ) system, an 8-channel National Instruments NI 9201 module, was employed for reading the voltage across the resistive load (which was also the voltage across the harvester). The NI modules were placed in an NI cDAQ 9172 chassis connected with a USB cable to the computer.

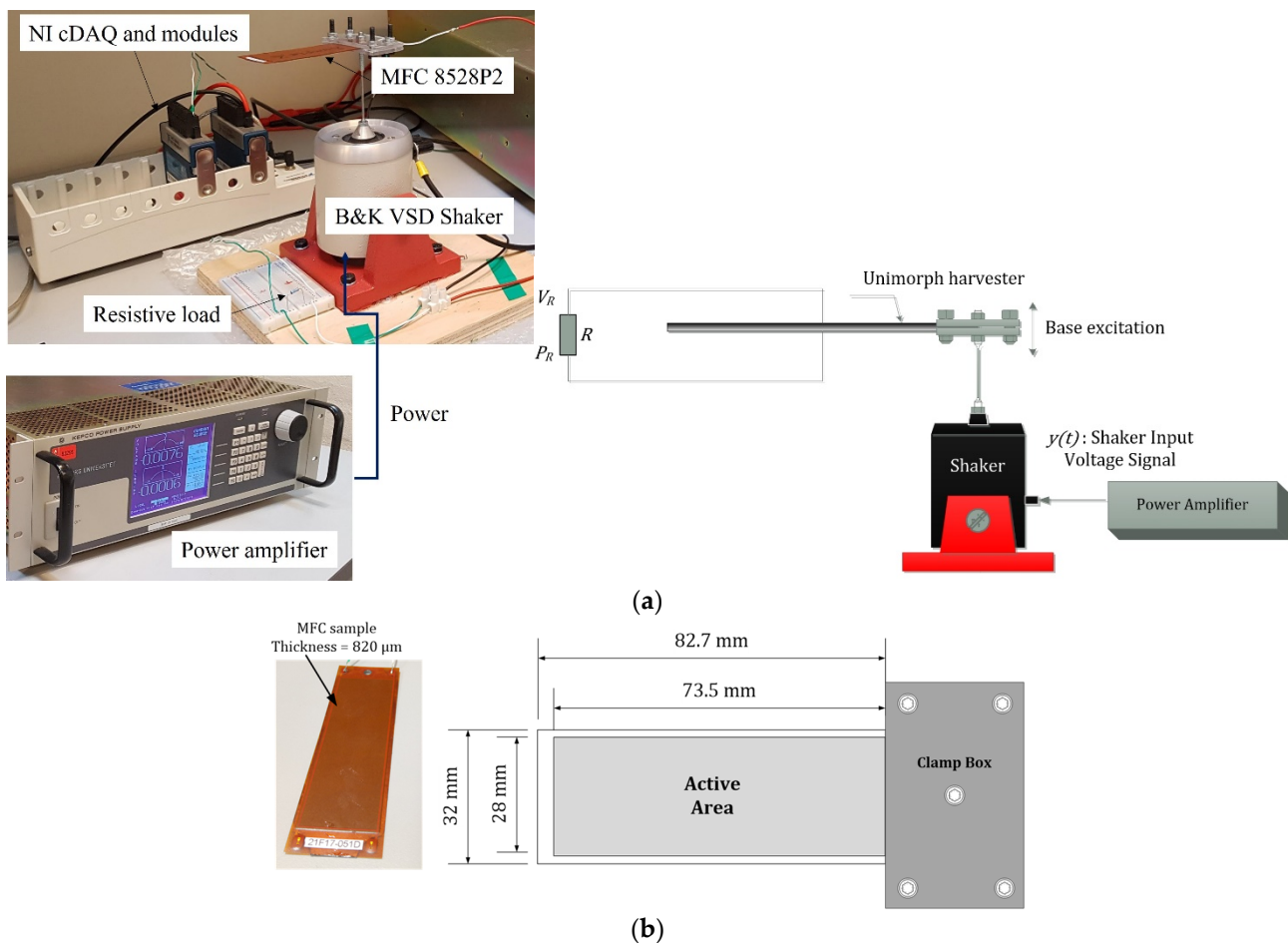


Figure 3. (a) Test rig and (b) MFC piezoelectric sample dimensions.

The shaker input voltage signal, $y(t)$, was varied in frequency and amplitude, and the piezoelectric voltage was measured. The shaker input voltage was a single-frequency or multiple-frequency harmonic.

The piezoelectric sample comprised a macro-fibre composite (MFC) of 0.3 mm in thickness, an aluminium substrate shim of 0.12 mm , and an epoxy rapid 332 bonding layer of $\sim 0.4 \text{ mm}$ in thickness. The bonding layer has little effect on the natural frequency, but it is a significant source of damping [26]. Therefore, the bonding layer was neglected in the structural modelling of the natural frequency; however, its effect was considered by extracting the damping coefficient experimentally, so the bonding layer influence was observed. The bonding layer joined the MFC and substrate shim. The MFC was the M-8528-P2 type from Smart Material GmbH (Dresden, Germany) [27], a piezoelectric bending energy harvester. The MFC had seven sub-layers: two Kapton outer layers, two acrylic

layers, two electrodes, and one central active piezoelectric layer. More information about the MFC can be obtained from Smart Material Inc. [27]. Figure 3b shows the MFC sample.

4.2. PVEH Device Optimum Characterisation

The piezoelectric sample was primarily analysed and characterised with the model and experimental tests presented in this subsection. The material properties for modelling were as follows: Young's moduli of MFC and aluminium layers were 15.85 [28] and 68.9 GPa, and the corresponding densities were 5540 and 2700 kg/m³. The damping coefficient was 5% [29]. The relative permittivity coefficient and piezoelectric constant d_{31} were 1800 and -170×10^{-12} C/N, respectively.

For this energy harvester, the first undamped natural frequencies obtained with the current model were compared with those of the experimental tests, as reported in Table 2. The natural frequency difference was 1.3 Hz. The higher-mode natural frequencies are also given in Table 2 and were employed in the multi-modal analysis. This difference in the natural frequencies can be linked to the non-uniform piezoelectric MFC; in practice, the commercial MFC sample had an active area where the piezoelectric material was placed, and on the outer areas, there were only Kapton layers. Including this non-uniformity would have required advanced piezoelectric beam modelling, which was beyond the scope of this paper. For detailed demonstration and modelling of an MFC, one can refer to [16].

Table 2. Comparison of undamped natural frequencies between the presented method and the experiment.

	Undamped Natural Frequencies ω_r (Hz)		
	Experiment	Current Method (Presented in Section 2)	Error (Hz)
First bending mode	20.4	21.7	1.3 Hz
Second bending mode	—	136.3	—
Third bending mode	—	381.5	—
Fourth bending mode	—	747.7	—
Fifth bending mode	—	1235.9	—

Piezoelectric unimorph harvesters are characterised by a natural frequency and optimum power generation. The studied harvester was first evaluated over a frequency range to obtain these conditions. Figure 4a shows power with load resistances over frequency. The resonant frequency was constant for all the load resistances and was equal to $\omega_{r=1} = 20.4$ Hz. This frequency was the first resonant frequency of the harvester. Moreover, there was another resonant frequency, $\omega_{pc} = 31.0$ Hz, associated with the piezoelectric structural effects, here called piezoelectric-coupled frequency. Second, output power versus load resistances were evaluated for optimum load resistance selection. Figure 4b shows output power versus load resistance at the resonant frequency. The optimal load resistance of 21.8 k Ω led to the highest power generation.

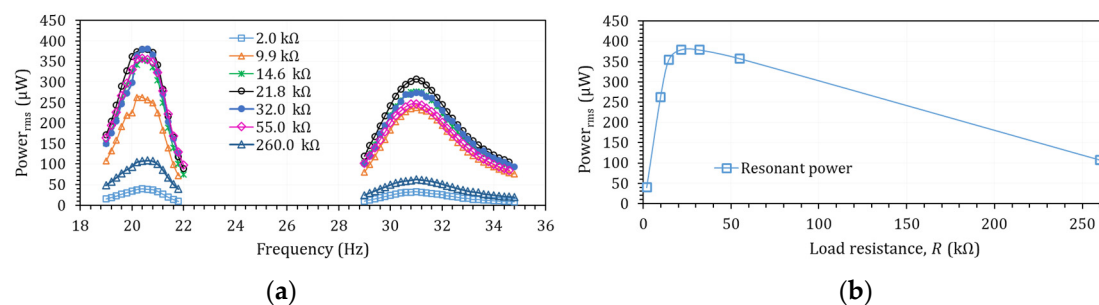


Figure 4. (a) Power versus frequency with different load resistances and (b) resonant output power for different loads.

5. Results and Discussion

The result section provides a comprehensive result set from the experimental tests. Through the experimental tests, power generation with $R_{\text{opt}} = 21.8 \text{ k}\Omega$ was studied with various excitation signals. Note that the load resistance of $R_{\text{opt}} = 21.8 \text{ k}\Omega$ was employed in all experimental results presented in this section. Excitation signals with Added White Gaussian Noise (AWGN), single-frequency harmonics, and multi-frequency harmonics were studied. Moreover, the effect of the vibration level from low-level to high-level vibrations was studied with harmonics with single frequency and multi-frequencies. Because in piezoelectric energy harvesting applications a harvester's natural frequency is matched to the dominant acceleration frequency, here, $\Omega = \omega_{r=1}$ was assumed.

5.1. Effects of Adding White Noise to the Excitation Signal

Pure analytical solutions often consider a single harmonic signal without noise as an excitation signal. In contrast, practical vibration sources often have added noise. Here, the effect of adding white noise was studied by considering Added White Gaussian Noise (AWGN) for a single harmonic signal with matched frequency, i.e., $\Omega = \omega_{r=1}$. The shaker vibration signal was $y(t) = 0.1(1 + \text{AWGN}) \sin(2\pi\Omega t)$ (V), where "AWGN" is the white noise percentage, 1% or 2%. The shaker vibration signals with and without AWGN are shown in Figure 5a. The output power results showed that adding white noise increased the power slightly (see Figure 5b). White noise, i.e., random noise with a uniform frequency domain value, caused additional vibration on the piezoelectric harvester, so power generation slightly increased. An important conclusion is that white noise in the practical vibration data did not show a reduction in power influence.

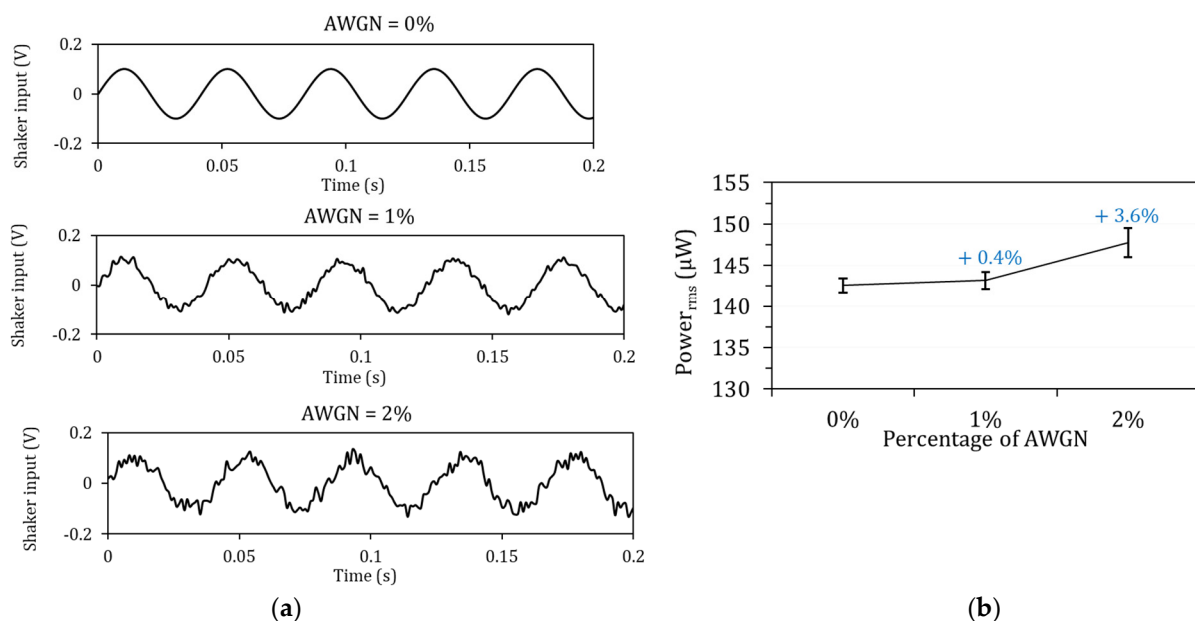


Figure 5. Effects of Added White Gaussian Noise (AWGN) on MFC power generation with fundamental natural frequency excitation: (a) shaker vibration signals and (b) RMS power with R_{opt} .

5.2. Effects of Increasing the Vibration Level with Single-Frequency Harmonics

A single-frequency harmonic excited the harvester, and the vibration-level effect on the output power was investigated by increasing the harmonic amplitude. This experimental setup tested the linearity assumption of power generation versus input square acceleration amplitude. Note that a single frequency does not imply constant frequency. Various single-frequency harmonics with different frequencies were studied. Considering the matched frequency ($\Omega_1 = \omega_{r=1}$) up to six harmonics, the natural multiples of the fundamental frequency were studied. Therefore, $\Omega_i = i \times \omega_{r=1}, i = 1, \dots, 6$.

Shaker input signals are symbolised with $y_{\mathcal{J}\mathcal{K}}(t) = Y_{\mathcal{J}}\sin(\mathcal{K}\omega_r t)$, where Y is the magnitude of the shaker excitation signal and \mathcal{K} is the driving frequency multiplier. Subscript \mathcal{J} denotes different excitation magnitude levels for one driving frequency. By changing Y , the vibration level moves from low-level to high-level vibrations; in other words, the strain on the piezoelectric material changes from low levels to high levels.

The output power with R_{opt} was recorded during three independent runs. Table 3 shows the output power, and average and experimental errors for all the harmonics and vibration levels. An experimental error of less than 4% implies experimental repeatability. The sensitivity comparisons showed the dramatic power increase obtained by magnifying the excitation amplitude of all excitation harmonics; however, the trends were not the same for all harmonics.

Table 3. Base excitation signal characteristics and experimental results obtained by connecting harvester to optimum load.

Ω_i	$Y_{\mathcal{J}}$ (V)	$P_{rms}(\mu W)$	Experimental Error (%)	Ω_i	$Y_{\mathcal{J}}$ (V)	$P_{rms}(\mu W)$	Experimental Error (%)
$\Omega_1 =$ $1 \times \omega_{r=1} = 20.4$ Hz	0.04	19.51	1.22	$\Omega_3 =$ $3 \times \omega_{r=1} = 61.2$ Hz	0.04	4.01	1.13
	0.05	38.25	1.25		0.05	6.36	0.33
	0.075	140.68	1.20		0.075	13.73	0.55
	0.09	243.13	1.54		0.09	19.45	0.49
	0.1	344.21	1.18		0.1	24.08	1.71
	0.12	543.71	0.29		0.04	3.01	2.75
	0.17	1104.92	0.29		$\Omega_4 =$ $4 \times \omega_{r=1} = 81.6$ Hz	0.05	4.87
0.2	1370.04	1.70	0.075	10.13		0.46	
0.04	6.98	1.76	0.09	14.32		0.81	
$\Omega_2 =$ $2 \times \omega_{r=1} = 40.8$ Hz	0.05	11.45	1.05	0.1	17.44	0.47	
	0.075	24.91	0.75	$\Omega_5 = 5 \times$ $\omega_{r=1} = 102.0$ Hz	0.05	4.34	3.26
	0.09	35	0.82		0.08	10.65	1.78
	0.1	43.45	0.58		0.1	17.25	3.85
	$\Omega_6 = 6 \times$ $\omega_{r=1} = 122.4$ Hz	0.05	3.84	2.32	0.05	3.84	2.32
0.08		9.2	0.96	0.08	9.2	0.96	
0.1		14.12	2.99	0.1	14.12	2.99	

Output power (P) versus square shaker signal amplitude (Y^2) for Ω_1 to Ω_6 frequencies are plotted in Figure 6a. According to the analytical model in Equation (9), the relation between power and square input amplitude is linear for all frequencies; however, Figure 6a demonstrates a separate pattern for Ω_1 excitation. This apparent pattern indicates that the resonant excitation frequency differed from the other frequencies.

Further analyses of the power pattern were conducted with the dimensionless study of power versus square vibration amplitude. The dimensionless study divided the parameters into the lowest-level vibration amplitude and power. The dimensionless power–vibration values for Ω_1 excitation frequency and for Ω_2 to Ω_6 excitation frequencies are plotted in Figure 6b and c, respectively.

As shown in Figure 6c, the slope of the fitted line for Ω_2 to Ω_6 harmonic excitation frequencies was approximately one; power linearly changed by the square of input acceleration at these frequencies. This conclusion is in line with the analytic model in Equation (9). In contrast, for Ω_1 frequency, where the excitation frequency was the fundamental natural frequency (Figure 6b), the slope of the fitted line was approximately three.

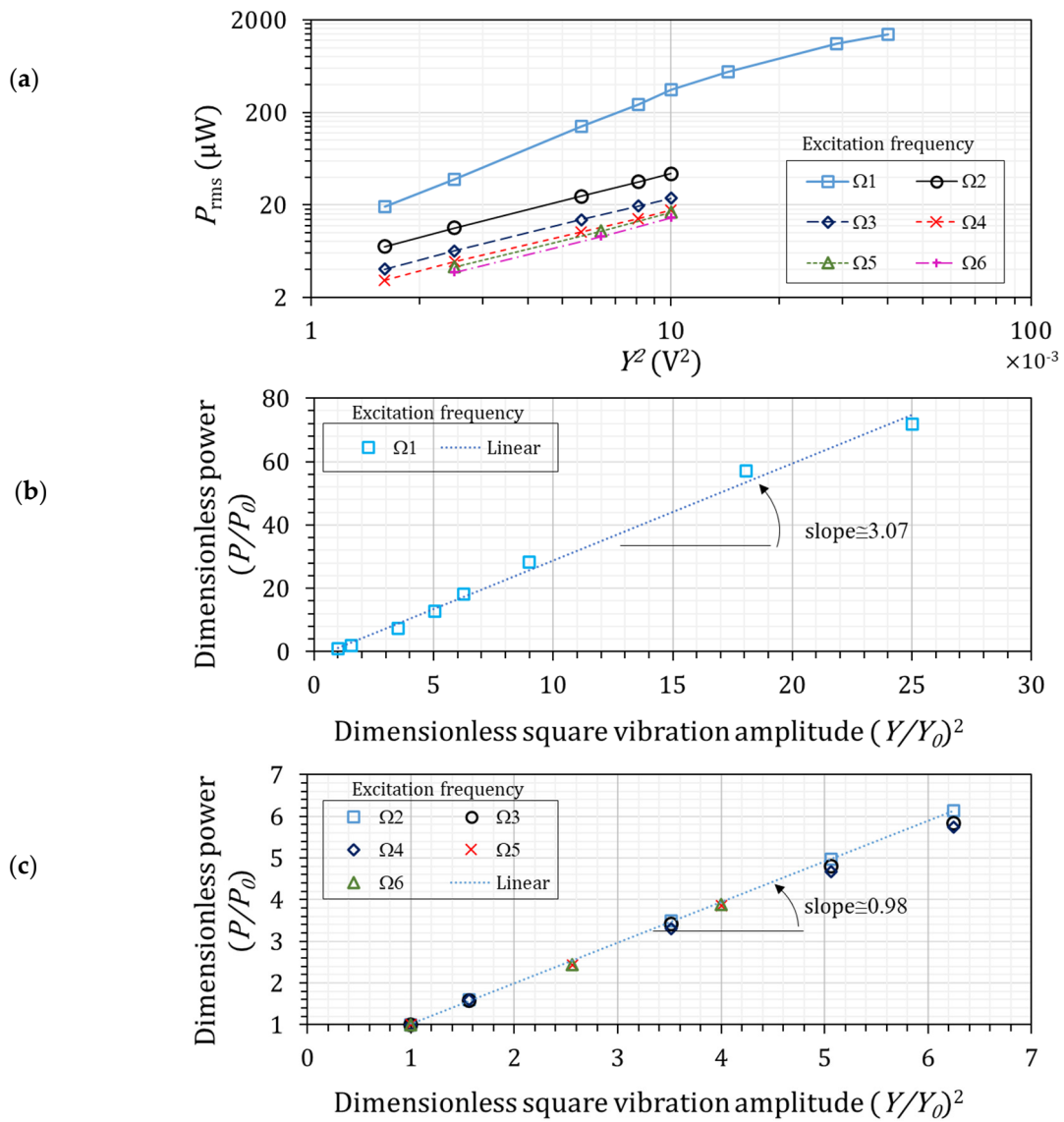


Figure 6. Power variation concerning excitation magnitude in the single-harmonic case with $R_{opt} = 21.8 \text{ k}\Omega$. (a) plots the output power (P) versus square shaker signal amplitude (Y^2) for W1 to W6 frequencies, (b,c) plot the dimensionless power–vibration values for W1 excitation frequency and for W2 to W6 excitation frequencies respectively.

According to the linear bending theory, the axial strain depends on the beam curvature [15], e.g., $\epsilon_{xx} \propto \frac{\partial^2 w}{\partial x^2}$. By increasing the vibration level, the strain on a piezoelectric material also increases. Assuming the matched frequency ($\Omega_1 = \omega_{r=1}$), Ω_1 -frequency vibration excitation creates resonance deformation on the piezoelectric beam, and the resonance deformation is large. Therefore, a high vibration level is expected to create elevated levels of strain, which goes beyond the linear assumption between the axial strain and beam curvature. However, the experimental dimensionless study showed that for higher harmonics, e.g., Ω_2 and beyond, a high vibration level does not cause a high strain level; therefore, the linear analytical model is valid.

It has been demonstrated that nonlinearity exists even in a typical no-added-tip-mass energy harvester. In many typical energy harvesters, an added mass adjusts the fundamental frequency and increases the power [30], inducing physical deformation, i.e., they become noticeably enlarged, at the acting frequency [31]. As observed in Figure 6b, increasing physical deformation creates nonlinearity, and the added-tip-mass effect is expected to enlarge nonlinearity. The tip mass affects the first vibration mode more substantially

than other vibration modes (because of the larger first-mode-shape magnitude); therefore, the added-tip-mass effect on the nonlinear effects of resonant excitation is expected to be considerable.

5.3. Effects of Increasing the Vibration Level with Multi-Frequency Harmonics

As demonstrated in Section 2, practical vibration energy sources only have single-frequency signals instead of a series of harmonic multipliers. Thus, a vibration-level study was carried out on a multi-harmonic signal using vibration-level control. The standard baseline excitation signal was the summation of harmonics with Ω_1 to Ω_6 frequencies, denoted by $Z_M(t)$; it excited the piezoelectric harvester, and the corresponding RMS power with optimum load was P_{Z_M} . $Z_M(t)$, as given in Equation (10) and shown in Figure 7a.

$$Z_M(t) = M[0.04 (V)]\sin(\Omega_1 t) + [0.05 (V)]\sin(\Omega_2 t) + [0.05 (V)]\sin(\Omega_3 t) + [0.05 (V)]\sin(\Omega_4 t) + [0.05 (V)]\sin(\Omega_5 t) + [0.05 (V)]\sin(\Omega_6 t) \tag{10}$$

where M is the signal magnification factor. Note that $\Omega_i = i \times \omega_{r=1}$, $i = 1, \dots, 6$. In practice, four magnification factors, $M = 1, 1.2, 1.5, 1.75$, and 2.0 , were assigned. The associated acceleration signals from $Z_1(t)$ to $Z_{M=2}(t)$ are shown in Figure 7b.

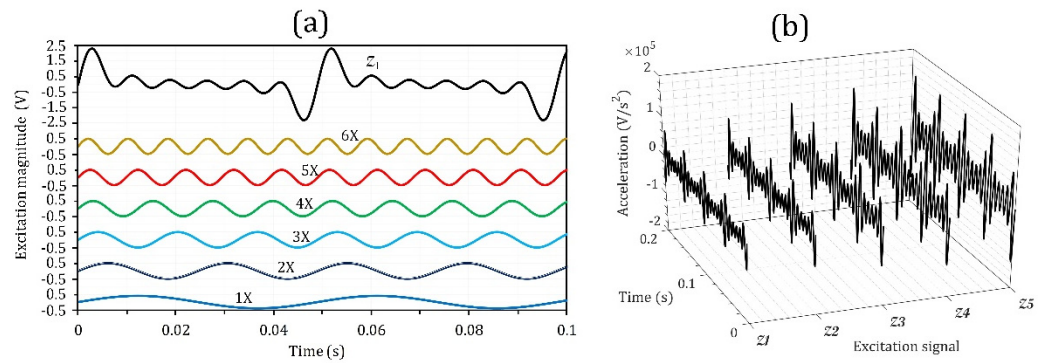


Figure 7. (a) Standard multi-harmonic base excitation signal and (b) applied acceleration for multi-harmonic base signals.

The optimum power with $21.8 \text{ k}\Omega$ for different magnification factors is shown in Figure 8a. As expected, the power increased with the increase in the excitation vibration level; however, a nonlinear variation was observed. Further analyses were conducted on dimensionless experimental power versus square magnification factor (Figure 8b). Figure 8b shows that the experimental correlation between P and M^2 was not linear, while according to the analytical modelling of $P \propto M^2$, the empirical correlation between power and the magnification factor is given by

$$\frac{P_{Z_M}}{P_{Z_1}} = 0.77 \ln M^2 \tag{11}$$

The output power obtained in the experiments was smaller than that obtained by employing the linear analytical theory. For explaining this statement, the interaction effects between the harmonics needed to be studied.

5.4. Interaction Effects between Different Excitation Harmonics

The interaction effects were studied by applying an excitation signal comprising six harmonics and controlling the harmonic amplitude. The excitation signal is denoted by

$$Z(t) = \alpha_1 \sin(\Omega_1 t) + \alpha_2 \sin(\Omega_2 t) + \alpha_3 \sin(\Omega_3 t) + \alpha_4 \sin(\Omega_4 t) + \alpha_5 \sin(\Omega_5 t) + \alpha_6 \sin(\Omega_6 t) \tag{12}$$

where α_1 to α_6 can be controllably changed. Note that $\Omega_i = i \times \omega_{r=1}$, $i = 1, \dots, 6$.

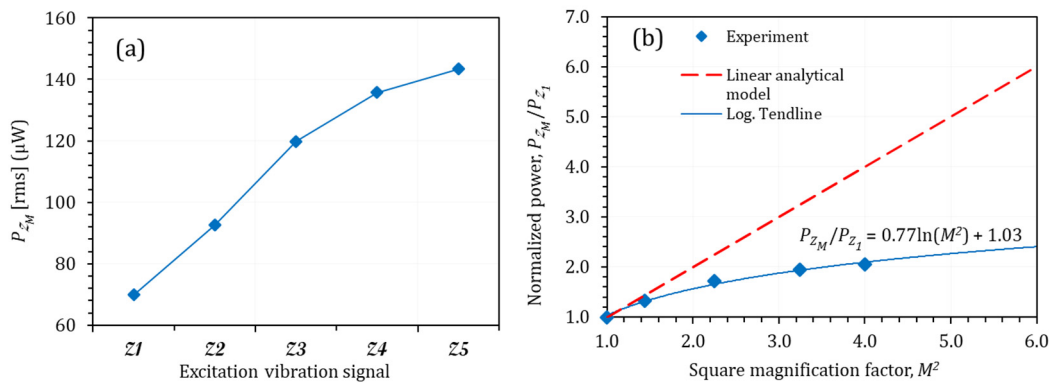


Figure 8. (a) Output power for different vibration-level multi-frequency excitation signals and (b) normalised power versus magnification factor.

A three-level experimental design was proposed so that nonlinear relationships could also be captured and the overlap of the interaction effects could be avoided. In addition, to avoid overlapping the interaction effects, two levels for α_1 and three levels for α_2 to α_6 were employed. A fractional factorial design using the orthogonal method of resolution III was used with 36 runs of experiments [32]. Table 4 shows the orthogonal array with thirty-six runs. Moreover, three duplications were performed.

Table 4. Orthogonal design of experiments on interaction effects of harmonics.

Index	α_1 (V)	α_2 (V)	α_3 (V)	α_4 (V)	α_5 (V)	α_6 (V)	Index	α_1 (V)	α_2 (V)	α_3 (V)	α_4 (V)	α_5 (V)	α_6 (V)
1	0.04	0.05	0.05	0.05	0.05	0.05	19	0.1	0.05	0.05	0.08	0.05	0.08
2	0.04	0.08	0.08	0.08	0.08	0.08	20	0.1	0.08	0.08	0.1	0.08	0.1
3	0.04	0.1	0.1	0.1	0.1	0.1	21	0.1	0.1	0.1	0.05	0.1	0.05
4	0.04	0.05	0.05	0.08	0.08	0.1	22	0.1	0.05	0.05	0.1	0.1	0.1
5	0.04	0.08	0.08	0.1	0.1	0.05	23	0.1	0.08	0.08	0.05	0.05	0.05
6	0.04	0.1	0.1	0.05	0.05	0.08	24	0.1	0.1	0.1	0.08	0.08	0.08
7	0.04	0.05	0.08	0.05	0.1	0.1	25	0.1	0.05	0.1	0.08	0.05	0.1
8	0.04	0.08	0.1	0.08	0.05	0.05	26	0.1	0.08	0.05	0.1	0.08	0.05
9	0.04	0.1	0.05	0.1	0.08	0.08	27	0.1	0.1	0.08	0.05	0.1	0.08
10	0.04	0.05	0.08	0.1	0.05	0.08	28	0.1	0.05	0.1	0.1	0.08	0.05
11	0.04	0.08	0.1	0.05	0.08	0.1	29	0.1	0.08	0.05	0.05	0.1	0.08
12	0.04	0.1	0.05	0.08	0.1	0.05	30	0.1	0.1	0.08	0.08	0.05	0.1
13	0.04	0.05	0.1	0.05	0.08	0.05	31	0.1	0.05	0.08	0.05	0.08	0.08
14	0.04	0.08	0.05	0.08	0.1	0.08	32	0.1	0.08	0.1	0.08	0.1	0.1
15	0.04	0.1	0.08	0.1	0.05	0.1	33	0.1	0.1	0.05	0.1	0.05	0.05
16	0.04	0.05	0.1	0.1	0.1	0.08	34	0.1	0.05	0.08	0.08	0.1	0.05
17	0.04	0.08	0.05	0.05	0.05	0.1	35	0.1	0.08	0.1	0.1	0.05	0.08
18	0.04	0.1	0.08	0.08	0.08	0.05	36	0.1	0.1	0.05	0.05	0.08	0.1

Table 5 shows the Analysis of Variance (ANOVA) table with which the meaningful variations were interpreted. Parameter F is the mean square of responses within the same treatment factor divided by the mean square of responses in all experimental runs. $F > 1$ indicates meaningful variation, and a greater F demonstrates a more sensitive treatment factor. The ANOVA table shows that variables α_1 to α_4 have $F > 1$, meaning that their influence on the output power was substantial. Table 5 shows that the influence of the α_1 factor (with Ω_1 frequency) was larger than that of the other factors and that the excitation frequencies of Ω_1 to Ω_4 had meaningful effects on the output power. This conclusion implies that harmonics in a practical vibration source up to the fourth harmonic should be considered.

Table 5. Analysis of Variance (ANOVA) table of the designed test with three duplications.

Variable	Standard Deviation of P_R	Degree of Freedom	Mean Square	F
α_1 (with Ω_1 frequency)	σ_{G_1}	1	$\sigma_{G_1} = 138,434.3$	$\sigma_{G_1} / (\sigma_e / 96) = 109.59$
α_2 (with Ω_2 frequency)	σ_{G_2}	2	$\sigma_{G_2} / 2 = 4418.2$	$(\sigma_{G_2} / 2) / (\sigma_e / 96) = 3.50$
α_3 (with Ω_3 frequency)	σ_{G_3}	2	$\sigma_{G_3} / 2 = 5538.2$	$(\sigma_{G_3} / 2) / (\sigma_e / 96) = 4.38$
α_4 (with Ω_4 frequency)	σ_{G_4}	2	$\sigma_{G_4} / 2 = 4964.7$	$(\sigma_{G_4} / 2) / (\sigma_e / 96) = 3.93$
α_5 (with Ω_5 frequency)	σ_{G_5}	2	$\sigma_{G_5} / 2 = 507.4$	$(\sigma_{G_5} / 2) / (\sigma_e / 96) = 0.40$
α_6 (with Ω_6 frequency)	σ_{G_6}	2	$\sigma_{G_6} / 2 = 119.5$	$(\sigma_{G_6} / 2) / (\sigma_e / 96) = 0.09$
Residual	σ_e	$3 \times 2^5 = 96$	$\sigma_e / 96 = 1263.2$	

Figure 9a–e demonstrate the interaction effects of different harmonics. The interaction effects of the Ω_1 – Ω_2 , Ω_1 – Ω_3 , and Ω_1 – Ω_4 harmonics were substantial, while the Ω_5 and Ω_6 harmonics had negligible effects. The charge cancellation effect of the Ω_1 – Ω_2 harmonics was visible, i.e., increasing α_2 (with Ω_2 frequency) adversely affected α_1 (with Ω_1 frequency) and increased the effect on power generation. In Ω_1 – Ω_3 and Ω_1 – Ω_4 harmonics, the interaction effects were positive. In other words, increasing α_3 (with Ω_3 frequency) or α_4 (with Ω_4 frequency) did not change the positive effect of the first harmonic.

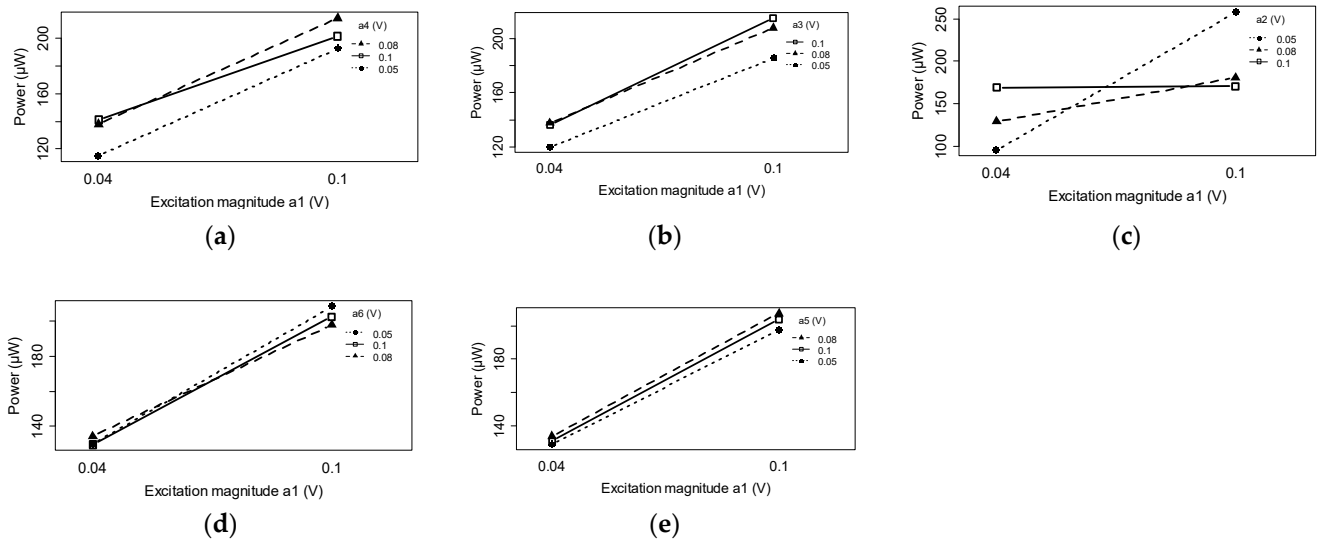


Figure 9. Interaction effects of different excitation harmonics in a multi-frequency excitation signal: (a) Ω_1 – Ω_4 effect; (b) Ω_1 – Ω_3 effect; (c) Ω_1 – Ω_2 effect; (d) Ω_1 – Ω_6 effect; (e) Ω_1 – Ω_5 effect.

The interaction study showed that the negative interaction between the Ω_1 harmonic and the Ω_2 harmonic led to smaller power generation than when applying the linear theory, which is observed in Figure 8b. This observation can be linked to the link between the resonant harvester frequencies and the different harmonics in the excitation signal. As demonstrated in Table 6, the first resonant frequency and the piezoelectric-coupled resonant frequency ($\omega_{r=1}$ and ω_{pc}) were in the range of the first and second excitation harmonics ($\Omega_{i=1}$ and $\Omega_{i=2}$). Thus, these two excitation harmonics are expected to have considerable effects compared with the effects of high harmonics.

Table 6. Comparison of the harvester’s resonant frequencies and the external excitation harmonic frequencies.

Harvester’s Resonant Frequencies	External Excitation Frequencies
$\omega_{r=1} = 21.7 \text{ Hz}$	$\Omega_{i=1} = 20.4 \text{ Hz}$
$\omega_{pc} = 31.0 \text{ Hz}$	$\Omega_{i=2} = 40.8 \text{ Hz}$
$\omega_{r=2} = 136.3 \text{ Hz}$	$\Omega_{i=3} = 61.2 \text{ Hz}$
$\omega_{r=3} = 381.5 \text{ Hz}$	$\Omega_{i=4} = 81.6 \text{ Hz}$
$\omega_{r=4} = 747.7 \text{ Hz}$	$\Omega_{i=5} = 102.0 \text{ Hz}$
$\omega_{r=5} = 1235.9 \text{ Hz}$	$\Omega_{i=6} = 124.4 \text{ Hz}$

5.5. Proposing a Nonlinear Model

Large-deformation strain and nonlinear stress–strain constitutive equations are proposed. Base excitation $a(t)$ deforms the piezoelectric beam with the deformation shape of $w(x, t)$. In a nonlinear framework, the axial strain is given by

$$\epsilon_{xx} = -z \frac{\frac{\partial^2 w(x,t)}{\partial x^2}}{\left(1 + \left(\frac{\partial w(x,t)}{\partial x}\right)^2\right)^{\frac{3}{2}}} \tag{13}$$

at level z from the neutral axis.

Moreover, the nonlinear stress–strain constitutive equations can be given by [33]

$$T_{xx}^p = Y_p \epsilon_{xx} - \bar{e}_{31} E_z + \frac{1}{2} \beta_p \epsilon_{xx}^2 \tag{14}$$

$$T_{xx}^s = Y_s \epsilon_{xx} + \frac{1}{2} \beta_s \epsilon_{xx}^2 \tag{15}$$

where T_{xx} is the axial stress, E_z is the z -component electrical field, and β is the nonlinear coefficient.

Thus, the internal bending moment can be calculated with

$$M(x, t) = -b \left(\int_{-z_a}^{-z_b} T_{xx}^s z dz + \int_{-z_b}^0 T_{xx}^p z dz + \int_0^{z_c} T_{xx}^p z dz \right) \tag{16}$$

Consequently, the beam stiffness (YI) and piezoelectric coupling coefficients (Y_r and Λ_r) are obtained for the nonlinear model.

The electromechanical voltage equation for the nonlinear model is given by

$$C_P \dot{V}_R(t) + \frac{1}{R} V_R(t) = -\frac{\bar{e}_{31}(h_p + h_s)b}{2} \int_0^L \frac{d}{dt} \left[\frac{\partial^2 w(x,t)}{\partial x^2} \left(1 + \left(\frac{\partial w(x,t)}{\partial x} \right)^2 \right) \right] dx \tag{17}$$

More details about the nonlinear model can be found in ref. [34].

6. Concluding Remarks and Future Works

This paper presents extensive experimental works aimed at practical PEH performance characterisation. Single-frequency harmonics with resonant and off-resonant excitation frequencies, and multi-frequency signals as practical vibration signals were studied as PVEH excitation signals. The investigations demonstrated the high-strain-level nonlinearities at resonance, while off-resonant harmonics followed the linear theories. Furthermore, with multi-frequency signals, resonance nonlinearity and different frequency interactions caused nonlinear performance in the PEH. This paper contributes to the realistic evaluation of piezoelectric energy harvesters. Nonlinear energy harvester models with more experimental investigation are proposed for future work. Moreover, further studies on

the parameters of the flexibility characteristics of energy harvesters, such as thickness and width, are needed.

Funding: Independent Research Fund Denmark International Post-doc grant under grant number 1031-00001B.

Data Availability Statement: Not applicable.

Acknowledgments: This research was partially financed by Independent Research Fund Denmark International Post-doc grant under grant number 1031-00001B.

Conflicts of Interest: The author declares no conflict of interest.

References

1. Khazaee, M.; Rosendahl, L.; Rezania, A. Online Condition Monitoring of Rotating Machines by Self-Powered Piezoelectric Transducer from Real-Time Experimental Investigations. *Sensors* **2022**, *22*, 3395. [[CrossRef](#)] [[PubMed](#)]
2. Ali, F.; Raza, W.; Li, X.; Gul, H.; Kim, K.H. Piezoelectric Energy Harvesters for Biomedical Applications. *Nano Energy* **2019**, *57*, 879–902. [[CrossRef](#)]
3. Sarker, M.R.; Julai, S.; Sabri, M.F.M.; Said, S.M.; Islam, M.M.; Tahir, M. Review of Piezoelectric Energy Harvesting System and Application of Optimization Techniques to Enhance the Performance of the Harvesting System. *Sens. Actuators A Phys.* **2019**, *300*, 111634. [[CrossRef](#)]
4. Sezer, N.; Koç, M. A Comprehensive Review on the State-of-the-Art of Piezoelectric Energy Harvesting. *Nano Energy* **2021**, *80*, 105567. [[CrossRef](#)]
5. Covaci, C.; Gontean, A. Piezoelectric Energy Harvesting Solutions: A Review. *Sensors* **2020**, *20*, 3512. [[CrossRef](#)]
6. Khazaee, M.; Rezania, A.; Rosendahl, L. Piezoelectric Resonator Design and Analysis from Stochastic Car Vibration Using an Experimentally Validated Finite Element with Viscous-Structural Damping Model. *Sustain. Energy Technol. Assess.* **2022**, *52*, 102228. [[CrossRef](#)]
7. Adhikari, S.; Friswell, M.I.; Inman, D.J. Piezoelectric Energy Harvesting from Broadband Random Vibrations. *Smart Mater. Struct.* **2009**, *18*. [[CrossRef](#)]
8. Zhang, Y.; Jiao, Z.; Duan, X.; Xu, Y. Stochastic Dynamics of a Piezoelectric Energy Harvester with Fractional Damping under Gaussian Colored Noise Excitation. *Appl. Math. Model.* **2021**, *97*, 268–280. [[CrossRef](#)]
9. Ambrozkiewicz, B.; Grabowski, L.; Czyż, Z.; Karpiński, P.; Staczek, P.; Litak, G. Ceramic-Based Piezoelectric Material for Energy Harvesting Using Hybrid Excitation. *Material* **2021**, *14*. [[CrossRef](#)]
10. Leland, E.S.; Wright, P.K. Resonance Tuning of Piezoelectric Vibration Energy Scavenging Generators Using Compressive Axial Preload. *Smart Mater. Struct.* **2006**, *15*, 1413–1420. [[CrossRef](#)]
11. Roundy, S.; Leland, E.S.; Baker, J.; Carleton, E.; Reilly, E.; Lai, E.; Otis, B.; Rabaey, J.M.; Wright, P.K.; Sundararajan, V. Improving Power Output for Vibration-Based Energy Scavengers. *IEEE Pervasive Comput.* **2005**, *4*, 28–36. [[CrossRef](#)]
12. Khazaee, M.; Rezaniakolaei, A.; Rosendahl, L.A. A Study on Interaction Effects of Different Harmonics in Translational Base Excitation for Piezoelectric Vibration Energy Harvesters. In Proceedings of the ECCOMAS Smart 2019, Paris, France, 8–11 July 2019.
13. Noel, A.B.; Abdaoui, A.; Elfouly, T.; Ahmed, M.H.; Badawy, A.; Shehata, M.S. Structural Health Monitoring Using Wireless Sensor Networks: A Comprehensive Survey. *IEEE Commun. Surv. Tutor.* **2017**, *19*, 1403–1423. [[CrossRef](#)]
14. Li, H.; Tian, C.; Deng, Z.D. Energy Harvesting from Low Frequency Applications Using Piezoelectric Materials. *Appl. Phys. Rev.* **2014**, *1*, 041301. [[CrossRef](#)]
15. Khazaee, M.; Rezania, A.; Rosendahl, L. An Experimental Study to Determine Damping of Piezoelectric Harvesters Using Transient Analysis of Unified Electromechanical Voltage Equation. *Energy Convers. Manag.* **2021**, *227*, 113567. [[CrossRef](#)]
16. Khazaee, M.; Rezaniakolaei, A.; Rosendahl, L. A Broadband Macro-Fiber-Composite Piezoelectric Energy Harvester for Higher Energy Conversion from Practical Wideband Vibrations. *Nano Energy* **2020**, *76*, 104978. [[CrossRef](#)]
17. Wei, C.; Jing, X. A Comprehensive Review on Vibration Energy Harvesting: Modelling and Realization. *Renew. Sustain. Energy Rev.* **2017**, *74*, 1–18. [[CrossRef](#)]
18. Roundy, S.; Wright, P.K.; Rabaey, J. A Study of Low Level Vibrations as a Power Source for Wireless Sensor Nodes. *Comput. Commun.* **2003**, *26*, 1131–1144. [[CrossRef](#)]
19. Khazaee, M.; Rezania, A.; Rosendahl, L. Effect of Damage and Support Damping Mechanisms on Unimorph Piezoelectric Energy Harvester. *J. Vib. Control* **2019**, 107754631985516. [[CrossRef](#)]
20. Evensen, D.A. Nonlinear Vibrations of Beams with Various Boundary Conditions. *AIAA J.* **1968**, *6*, 370–372. [[CrossRef](#)]
21. Safaei, M.; Sodano, H.A.; Anton, S.R. A Review of Energy Harvesting Using Piezoelectric Materials: State-of-the-Art a Decade Later (2008–2018). *Smart Mater. Struct.* **2019**, *28*. [[CrossRef](#)]
22. Khazaee, M.; Rezaniakolaei, A.; Moosavian, A.; Rosendahl, L. A Novel Method for Autonomous Remote Condition Monitoring of Rotating Machines Using Piezoelectric Energy Harvesting Approach. *Sens. Actuators A Phys.* **2019**, *295*, 37–50. [[CrossRef](#)]

23. Jovanović, D.; Raos, M.; Jovanović, M.; Stanković, M.; Živković, L.; Protić, M. Vibration Analysis of the Boiler Supply Air Fan—A Case Study. *Springer Proc. Phys.* **2018**, *198*, 227–237. [[CrossRef](#)]
24. Yang, P.; Yuan, Q.; Huang, C.; Zhou, Y.; Li, H.; Zhou, Y. Analysis of the Impacts of Bearing on Vibration Characteristics of Rotor. *Shock Vib.* **2017**, *2017*, 8098591. [[CrossRef](#)]
25. Khazaei, M.; Huber, J.E.; Rosendahl, L.; Rezaei, A. The Investigation of Viscous and Structural Damping for Piezoelectric Energy Harvesters Using Only Time-Domain Voltage Measurements. *Appl. Energy* **2021**, *285*, 116427. [[CrossRef](#)]
26. Khazaei, M.; Huber, J.E.; Rosendahl, L.; Rezaei, A. On the Determination of Viscous and Structural Damping Coefficients for Piezoelectric Energy Harvesters Using Only Time-Domain Voltage Measurements. *Appl. Energy* **2021**, *285*, 116427. [[CrossRef](#)]
27. Smart Material GmbH Company, Dresden, Germany. Available online: <https://www.smart-material.com/13CompOverviewV2.html> (accessed on 9 December 2022).
28. Smart Materials Datasheet. Available online: <https://www.Smart-Material.Com> (accessed on 9 December 2022).
29. Khazaei, M.; Rezaniakolaei, A.; Rosendahl, L. An Experimental Study on Macro Piezoceramic Fiber Composites for Energy Harvesting. *Mater. Sci. Forum* **2019**, *951 MSF*, 3–8. [[CrossRef](#)]
30. Yi, J.W.; Shih, W.Y.; Shih, W.H. Effect of Length, Width, and Mode on the Mass Detection Sensitivity of Piezoelectric Unimorph Cantilevers. *J. Appl. Phys.* **2002**, *91*, 1680–1686. [[CrossRef](#)]
31. Kim, M.; Hoegen, M.; Dugundji, J.; Wardle, B.L. Modeling and Experimental Verification of Proof Mass Effects on Vibration Energy Harvester Performance. *Smart Mater. Struct.* **2010**, *19*, 045023. [[CrossRef](#)]
32. Lawson, J. *Design and Analysis of Experiments with R*; CRC Press: Boca Raton, FL, USA, 2014; ISBN 9781498728485.
33. Abdelkefi, A.; Nayfeh, A.H.; Hajj, M.R. Effects of Nonlinear Piezoelectric Coupling on Energy Harvesters under Direct Excitation. *Nonlinear Dyn.* **2012**, *67*, 1221–1232. [[CrossRef](#)]
34. Firoozy, P.; Khadem, S.E.; Pourkiaei, S.M. Power Enhancement of Broadband Piezoelectric Energy Harvesting Using a Proof Mass and Nonlinearities in Curvature and Inertia. *Int. J. Mech. Sci.* **2017**, *133*, 227–239. [[CrossRef](#)]

Disclaimer/Publisher’s Note: The statements, opinions and data contained in all publications are solely those of the individual author(s) and contributor(s) and not of MDPI and/or the editor(s). MDPI and/or the editor(s) disclaim responsibility for any injury to people or property resulting from any ideas, methods, instructions or products referred to in the content.